# Mechanical Properties and Linear Infrared Dichroism of Thin Films of Polyurethane Nanocomposites

**Lahorija Bistričić,[1] Mirela Leskovac,[2] Goran Baranović,[3] Sanja Lučić Blagojević[2]**

[1]*Department of Applied Physics, Faculty of Electrical Engineering and Computing, University of Zagreb, Unska 3, 10000 Zagreb, Croatia*
[2]*Faculty of Chemical Engineering and Technology, University of Zagreb, Marulićev trg 19, 10000 Zagreb, Croatia*
[3]*Rugjer Bošković Institute, P.O. Box 1016, 10001 Zagreb, Croatia*

Received 14 September 2007; accepted 15 November 2007
DOI 10.1002/app.27754
Published online 11 January 2008 in Wiley InterScience (www.interscience.wiley.com).

**ABSTRACT:** Morphological, mechanical, and Fourier transform infrared dichroic investigations were performed on neat polyurethane (PU) polymer matrix and PU+$CaCO_3$ nanocomposite thin films to determine how the nanofiller influenced the mechanical properties. The measurements were performed on strips that were cut from the prepared films in parallel and perpendicular directions with respect to the direction of film preparation. Optical microscopy of PU and the PU+$CaCO_3$ nanocomposite revealed the strain-induced transition from a continuous spherulitic morphology to a fiberlike structure. The stress–strain behavior of the neat PU and PU+$CaCO_3$ nanocomposite films showed significant differences at large strain regimes. The experimental results suggest that the mechanical properties were strongly related to the orientational behavior of the separated phases. The orientation of the hard and soft segments was analyzed by the orientation function calculated from the IR absorbances. A correlation between the orientations of segments, tensile properties, and hardness of the investigated polymer films was established. © 2008 Wiley Periodicals, Inc. J Appl Polym Sci 108: 791–803, 2008

**Key words:** FT-IR; nanocomposites; orientation; phase separation; polyurethanes

## INTRODUCTION

Polyurethanes (PU) are very attractive materials for investigations because of their specific structure, which consists of flexible (soft) and stiff (hard) segments. They are also very promising in many different fields, such as optoelectronics, shape-memory materials, conducting polymers, and biotechnology. Thermodynamic incompatibility between the soft and hard segments causes microphase separation. The domain morphology in such phase-separated structures achieved by phase separation or phase mixing has a great influence on the PU properties.[1] A hard-segment phase reinforces the soft-segment phase by acting as a set of filler particles dispersed in the soft-segment phase. Hard-segment domains at room temperature strongly influence the physical characteristics of PU copolymers.[2] Most hard segments in hard domains are physically connected to each other through hydrogen bonding or van der Waals interaction forces.

The physical properties of PU depend strongly upon the degree of alignment of the segments in polymeric chain. Properties such as tensile strength, Young's modulus, and toughness all correlate with the degree of chain orientation. IR linear dichroism measurements are suitable for studying the behavior of a multicomponent system because the orientation of the different components can be distinguished. In PU, the different domain behavior can be monitored with characteristic IR vibrational bands for functional groups.

Recently, inorganic–organic composite materials have attracted great attention because they exhibit properties much superior to conventional materials.[3–10] Polymer-based nanocomposites are formed by the dispersion of inorganic nanofillers (e.g., silica, titanium oxide, carbon nanotubes) into the organic polymer matrix. These systems combine the advantages of organic polymers, such as toughness and flexibility, with those of inorganic components, such as high heat resistance and good optical and mechanical properties.[3,4,5,11] Polymer-based nanocomposites exhibit remarkable improvements in mechanical, dielectric, magnetic, thermal optical, and acoustic properties compared to pure organic polymers.[3,4,5,11]

An understanding of how stress is transferred between the hard phase and matrix materials (soft phase) is important for the design of PU polymer nanocomposites with certain desired mechanical properties. Therefore, in this study, morphological, mechanical, and Fourier transform infrared (FTIR) investigations were performed on the neat PU polymer matrix and PU+$CaCO_3$ nanocomposite. Because

*Correspondence to:* L. Bistričić (lahorija.bistricic@fer.hr).

the mechanical properties of nanocomposites depend on the adhesion between the filler and the matrix and also on the distribution of nanoparticles in the matrix, in our previous study, we investigated the effects of the addition and pretreatment of $CaCO_3$ nanofiller on the properties of PU composites.[12] Scanning electron microscopy micrographs indicated a homogeneous distribution of nontreated $CaCO_3$ nanofiller in the PU matrix in the form of a netlike structure. The failure mechanisms were analyzed with scanning electron micrographs taken at the fracture surface of samples after the application of tensile stress at break ($\sigma_R$). The major mechanism in the neat PU matrix turned out to be shear yielding. The addition of the nanofiller improved the adhesion properties of the PU matrix because, in the PU+$CaCO_3$ nanocomposite, the failure occurred through the mechanisms of both dewetting and matrix shear yielding. The tensile properties of the PU+$CaCO_3$ nanocomposites were also investigated for dependence on the volume fraction of the filler. The maximum $\sigma_R$ was obtained at a 6% volume fraction of filler. On the basis of these results, in this study, we analyzed only the films containing 6% volume fraction of nanoparticles. The measurements were performed on strips that were cut from the prepared films in the longitudinal and transversal directions with respect to the direction of film preparation. In this study, we examined how the thickness of a film sample, stretching direction, and addition of nanofiller influenced the mechanical properties. The morphological and tensile properties of the PU and PU+$CaCO_3$ films were determined at the molecular level with a comprehensive IR dichroism study. The IR dichroism method was successfully applied to monitor the orientation and hydrogen bonding of different segments of PU.

## EXPERIMENTAL

### Materials

PU pellets (Desmocoll 620, commercial product of Bayer (Pittsburg, USA), predominantly linear hydroxyl PU based on bifunctional polyesters and diisocyanates with a high crystallization rate and low thermoplasticity) were used for the preparation of all samples in this study. A precipitate nano-$CaCO_3$ with a primary particle size of 80 nm, a specific surface area of 20 $m^2/g$, and a density of 2.73 $g/cm^3$ provided by Solvay (Rheinberg, Germany) was used as a filler in the PU nanocomposite.

### Preparation of the PU composites

The PU matrix and composite were prepared from a solution in acetone with concentration of 15 wt % solids. A composite was prepared with the addition of 6 vol % nano-$CaCO_3$. The solution was cast onto the polyethylene foil to a uniform thickness with a hand coater (designed to provide a predetermined film thickness). The samples were dried at room temperature to a constant weight. The final thicknesses of the prepared films were approximately 20 μm ($PU_{20}$) and 30 μm ($PU_{30}$ and PU+$CaCO_3$).

### Optical microscopy

Optical microscopy measurements were carried out on thin films with a light microscope (Leica Wetzlar, Germany, model DMLS) in transmission mode under parallel and crossed polarizers. A digital camera (Olympus) connected to a computer was used to capture the microscopy images.

### Mechanical properties

Mechanical measurements were performed on a Zwick universal testing machine (model 1445) (GrubH, Ulm, Germany) in uniaxial tension mode at 23°C and 65% relative humidity. Mechanical measurements were performed on strips of $PU_{30}$ and PU+$CaCO_3$ that were cut in the longitudinal and transversal directions to the axis of film preparation. Mechanical measurements were performed only on the 30 μm thick films due to the difficulties in placement of the 20 μm films in grips.

#### Tensile test measurements

Tensile tests were performed at a constant strain (ε) rate of 10 mm/min and a gauge length of 40 mm. The results are shown as stress versus ε curves.

#### Stress relaxation measurements

The specimens were extended to different ε levels, from 25 to 200% (with steps of 25% per interval) at a constant ε rate of 10 mm/min. When the appropriate ε was reached, it was maintained, and the stress was recorded for a time interval of 1300 s. Further extension of specimen was performed on the previously extended specimen. The results are shown as stress versus time stress relaxation plots.

### IR measurements

For IR measurements, the PU films were cut in strips with dimensions of 20 × 10 $mm^2$. The stretching of the samples was performed manually with an extensor in 5-mm steps starting from the initial length of 20 mm. The IR dichroic measurements were performed on strips that were cut in the longitudinal and transversal directions to the film axis preparation.

The FTIR spectra of the neat $PU_{20}$, $PU_{30}$, and $PU+CaCO_3$ nanocomposite films were recorded in a 4000–400-$cm^{-1}$ frequency region with an ABB Bomem (Quebec Canada) MB 102 spectrometer. The extensor containing the stretched sample was placed in the spectrometer. A ZnSe IR polarizer placed in front of the sample was used to produce an incident beam of parallel and perpendicular polarization to the stretching direction. The two spectra, $A_p(\tilde{v})$ and $A_n(\tilde{v})$, were collected with a resolution of 4 $cm^{-1}$ by coaddition of the results of 10 scans. The spectra were always collected from a sample that was first stretched and then kept at the given length for 20 min to allow for relaxation in the stretched state. A referent spectrum was collected before each measurement. To provide data on the polymer stress relaxation, several spectra were recorded immediately after stretching and then again 20 min later.

## RESULTS AND DISCUSSION

### Optical microscopy

Polymer materials are evaluated by microscopy techniques to determine their morphology and to provide an understanding of their structure–property relations.[13] The polarized micrographs of the unstretched thin films of neat $PU_{30}$ and the $PU+CaCO_3$ nanocomposite with 6 vol % $CaCO_3$ filler are shown in Figure 1. A polarization micrograph of the neat $PU_{30}$ polymer reveals a continuous spherulitic morphology with radial spherulites that impinged each other by growing during the crystallization process. Because of the occurrence of the polygonal spherulite forms, the maximal anisotropic diameter of the spherulites was measured on several polarization micrographs of the $PU_{30}$ sample, and the average spherulite diameter was about 40 μm.

The addition of filler particles into the PU matrix significantly influenced the coarse morphology. A substantial decrease in the spherulites size up to fine spherulitic or even grain morphology was observed with the incorporation of nano-$CaCO_3$ in the PU matrix [Fig. 1(A)]. The observed changes in the spherulite morphology were explained by the assumption that nano-$CaCO_3$ particles acted as nucleating agents in the crystallization process of the PU matrix and, thus, increased the heterogeneous nuclei density and decreased the spherulite size. Manias et al.[14] emphasized a somewhat different approach, which explains changes in spherulite morphology due to a nanofiller addition. The decrease in the spherulite size originates from a discontinuity of space caused by the filler particles, which forces the spherulites to have sizes comparable with the particle–particle separation, independent of the bulk polymer spherulite size. Moreover, this hypothesis also implies that the incorporation of nanoparticles in the semicrystalline polymer matrix might affect the crystallization of the polymer in different ways, depending on the polymer/filler interaction. The micrographs of neat $PU_{30}$ and the $PU+CaCO_3$ nanocomposites did not reveal any orientation effect at the microlevel that would depend on the film axis preparation. The polarized micrographs of neat $PU_{30}$ and the $PU+CaCO_3$ nanocomposite uniaxially stretched to a definite ε are shown in Figure 1(B,C). The neat $PU_{30}$ polymer stretched to 200% [Fig. 1(B)] clearly shows a deformation of spherulites to a stripedlike morphology due to the fibrillization of the PU matrix along the ε direction. A further increase in ε to 400% [Fig. 1(C)] resulted in denser and more highly oriented fibrils of the elongated $PU_{30}$ film that exhibited a lower transparency in the microscope. Christenson et al.[15] explained that the microfibrilar structure of stretched PU elastomers resulted from the reorganization of hard segments into domains that were separated by extended soft-segment domains. During the stretching of the neat $PU_{30}$ polymer, chromatization of sample was observed. The broad spectra of colors indicated different refractive indices of differently orientated fibrilar crystals.[13]

During the composite stretching, stress whitening of the composite sample was observed. Because of the stretching to 200 and 400%, the $PU+CaCO_3$ nanocomposite exhibited a finer morphology with shorter and thinner fibrils than did neat $PU_{30}$ as a consequence of decreased spherulite size [Fig. 1(B,C)]. That the orientation of filler particles followed the fibril orientation was also visible.

We expected that due to observed differences in morphology, the addition of filler would influence the mechanical properties.

### Mechanical properties

#### Tensile properties

The stress–ε curves of the neat $PU_{30}$ polymer and $PU+CaCO_3$ nanocomposite films are shown in Figure 2, and the tensile data are presented in Table I. Although both the neat $PU_{30}$ and $PU+CaCO_3$ nanocomposite films exhibited typical ductile behavior, they showed some differences in stress–ε behavior. The stress–ε curves initially exhibited an elastic region, yielding, and a plateau region (cold drawing) followed by an increase in stress due to ε-induced hardening, and finally, a failure occurred at high elongations. At low deformations, neat $PU_{30}$ and the $PU+CaCO_3$ nanocomposite showed similar behaviors with a necking area and a yield point in the stress–ε curves (Fig. 2). The initial response to stress was elastomeric stretching of the soft-segment matrix and rotation of the hard domains as rigid units toward

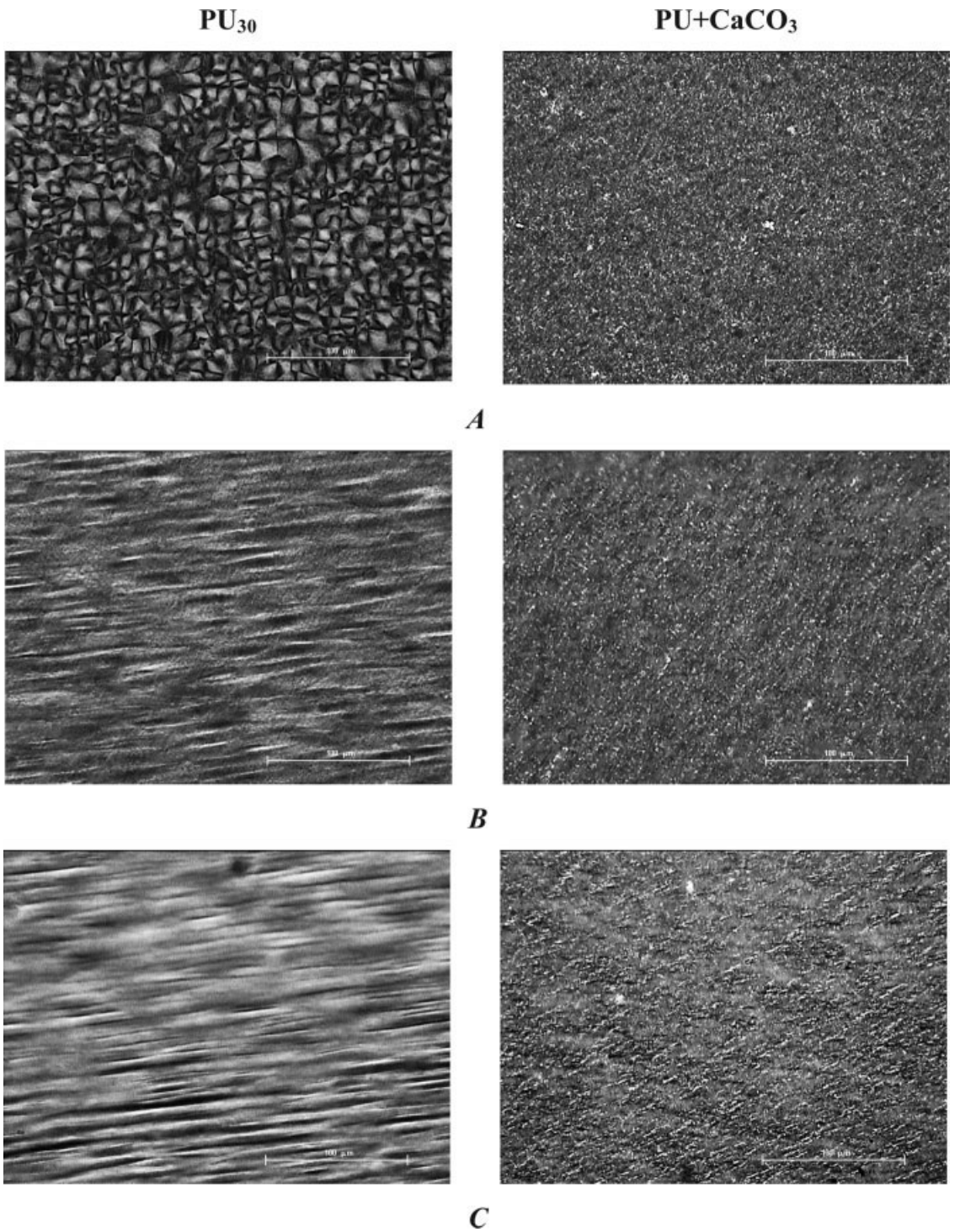


**Figure 1** Polarized micrographs of neat $PU_{30}$ and the PU+$CaCO_3$ nanocomposite: (A) unstretched, (B) stretched to 200%, and (C) stretched to 400%. Magnification = 200×.

the ε direction.[14] With the incorporation of the nano-$CaCO_3$ filler, the yield stress ($\sigma_y$) did not change markedly compared to the neat $PU_{30}$ polymer.

According to tensile results (Table I), the higher Young's modulus of the neat $PU_{30}$ polymer compared to the PU+$CaCO_3$ nanocomposite implied a higher stiffness in the unfilled polymer matrix. Generally, filler addition increases the polymer matrix modulus. The lower Young's modulus of the PU nanocomposite should have been a consequence of changes in the morphology observed in the polarized micrographs (Fig. 1). According to Tanniru and Misra,[16] an increase in spherulite size or an increase in crystallinity increases the modulus because large spherulites

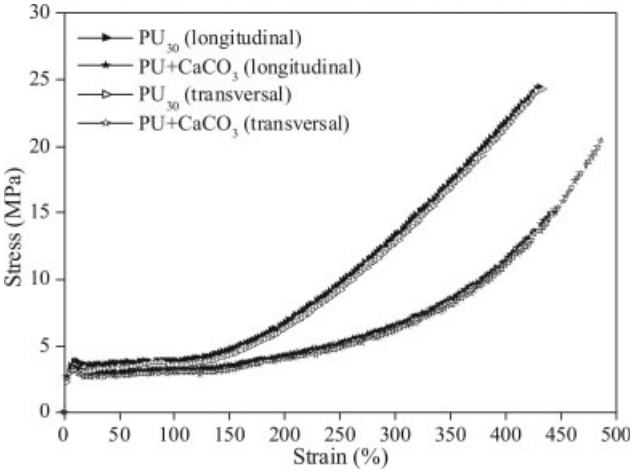


**Figure 2** Stress–ε curves of neat $PU_{30}$ and the $PU+CaCO_3$ nanocomposite stretched in the longitudinal and transversal directions of film preparation.

are able to resist higher loads. Those results are in accordance to the higher modulus of neat PU with a coarse spherulite morphology [Fig. 1(A)]. The yield point and cold drawing (plateau) corresponded with major, local morphological changes in the sample. Significant differences between $PU_{30}$ and the $PU+CaCO_3$ nanocomposite were observed at a large ε regime after cold drawing (i.e., after plateau region where the stress remained constant and the polymer was drawn into a thin neck) at ε's above 125%. For the neat $PU_{30}$ polymer matrix, ε-induced hardening occurred at relatively low ε's, around 125%, and then steeply increased. ε hardening in the segmented PUs depended in a very complex way on the hard-phase properties as well as on the soft-phase properties. The hard domains strengthened the polymer matrix by increasing the dissipation of energy, deflection and bifurcation of cracks, and cavitations and plastic deformation of domains. The soft phase influenced the hardening by the viscoelastic dissipation of energy near the crack tips, ε-induced crystallization, and development of high deformation.[17]

The incorporation of nano-$CaCO_3$ particles especially caused a significant decrease in ε-induced hardening. According to the tensile results, it was not possible to distinguish through which processes filler particles influenced the decrease in ε hardening of the polymer matrix.

According to the polarized micrograph, the morphologies of the stretched neat $PU_{30}$ and $PU+CaCO_3$ differed significantly. It is possible that the finer fibrillar structure of the stretched $PU+CaCO_3$ nanocomposite had a different ability for stress transfer, which was reflected in a lower tensile strength and extensibility. Additionally, during the $PU+CaCO_3$ nanocomposite stretching, stress whitening of the composite sample was observed, which thus implied a different mechanism of deformation of neat $PU_{30}$ and $PU+CaCO_3$. The polymer matrix predominantly displayed a shear bending mechanism, whereas $PU+CaCO_3$ additionally showed a crazing mechanism, which involved the formation of microcracks visible as stress whitening.[18] As shown in Table I, the work to break ($W_b$) of the neat $PU_{30}$ polymer matrix was higher than that of the $PU+CaCO_3$ nanocomposite, which indicates a higher toughness of the $PU_{30}$ matrix.

## Stress relaxation

When subjected to constant deformation, polymers typically exhibit a time-dependent relaxation behavior. Such phenomenon can be followed via stress relaxation.[12] Stress relaxation curves of neat $PU_{30}$ and the $PU+CaCO_3$ nanocomposite obtained by different ε levels in the longitudinal and transversal directions are shown in Figure 3. Although tensile measurements showed that there were no differences in the stress–ε curves depending on the direction of stretching, the stress relaxation measurements revealed substantial differences for both $PU_{30}$ and the $PU+CaCO_3$ nanocomposite samples (Fig. 3). It was evident that different curves relaxed to different plateau values, which referred to the residue stress different from zero. The rate of relaxation and residue stress of the longitudinally stretched specimens were lower than those of the transversally stretched specimens.

The neat $PU_{30}$ stretched in the longitudinal direction exhibited very extensive stress relaxation (Fig. 3). The $PU_{30}$ matrix revealed low residue stress in the longitudinal direction, especially at lower ε levels (25–100%). Further stretching above 125% resulted in higher residue stress as a consequence of structural changes. The stress relaxation and higher residue stress were ascribed to ε-induced processes that were not recoverable as orientation of hard

**TABLE I**
**Mechanical Properties of Neat $PU_{30}$ and the $PU+CaCO_3$ Nanocomposite**

| Sample | | $\sigma_y$ (MPa) | Secant modulus (MPa) | $\sigma_R$ (MPa) | Strain at break (%) | $W_b$ (Nm) |
|---|---|---|---|---|---|---|
| Longitudinal | $PU_{30}$ | 3.87 | 52.58 | 24.8 | 444.5 | 1.02 |
| | $PU+CaCO_3$ | 3.52 | 43.07 | 15.2 | 445.0 | 0.49 |
| Transversal | $PU_{30}$ | 3.46 | 46.22 | 24.5 | 431.7 | 1.23 |
| | $PU+CaCO_3$ | 3.29 | 40.22 | 20.6 | 486.8 | 0.55 |

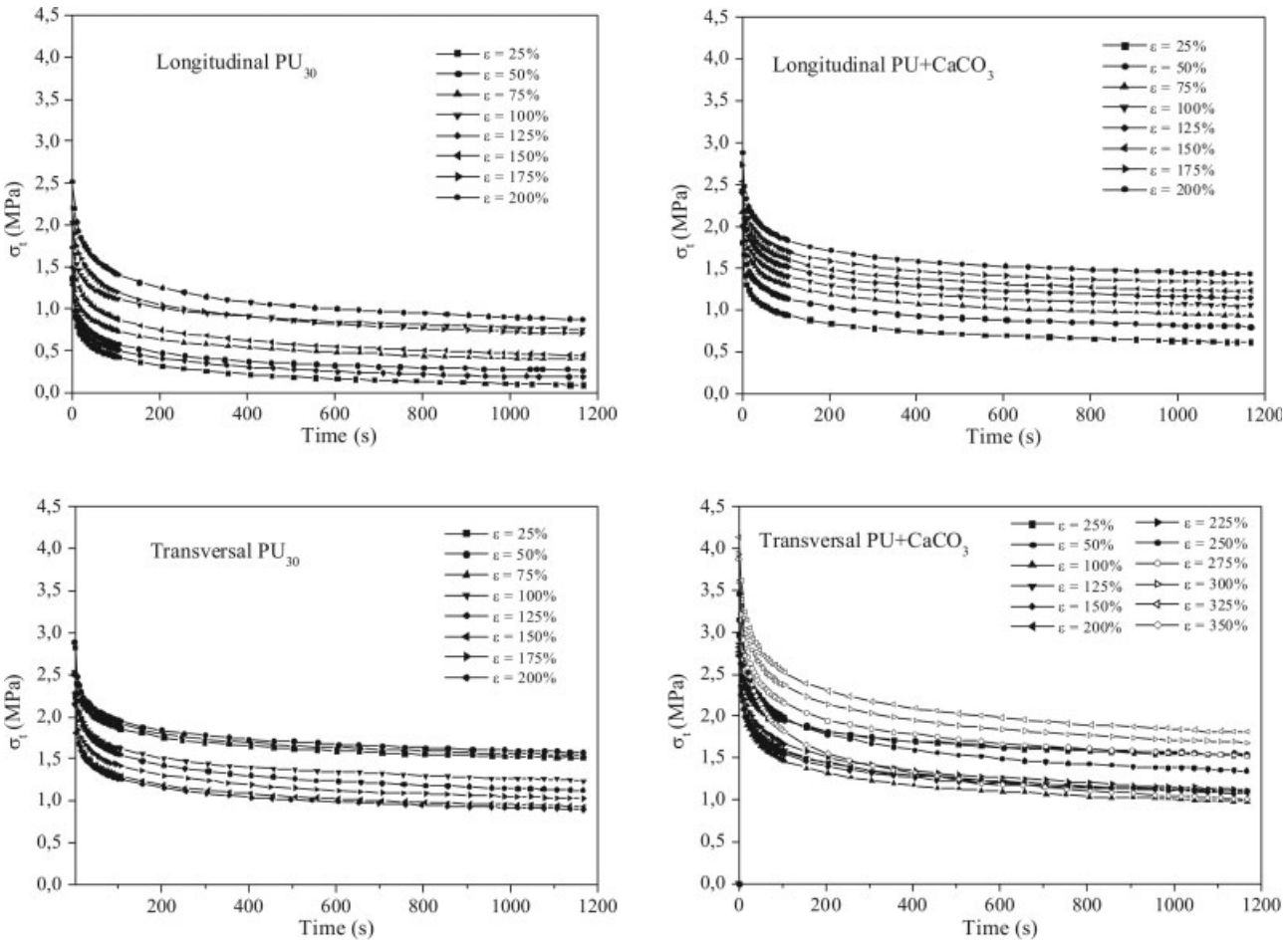


**Figure 3** Stress relaxation curves of the neat $PU_{30}$ and $PU+CaCO_3$ nanocomposite films at different ε levels. $\sigma_t$ is stress.

segments.[17] That was consistent with the tensile test results, where ε-hardening was observed at about 125% ε. The $PU_{30}$ matrix measured in the transversal direction showed a substantial decrease in the stress relaxation after 125% ε, with initially (at a ε range of 25–75%) higher residue stresses [Fig. 3(A)]. That suggests a weaker structure in the transversal direction, probably due to the inability of soft segments to elongate along the ε direction and to provide ε-induced hardening and chain relaxation. The results of the stress relaxation of the $PU_{30}$ matrix in the longitudinal and transversal directions indicate that the orientation of the soft segments was less developed in the transversal direction, which led to a lower degree of relaxation in this direction. The stress relaxation of $PU+CaCO_3$ was slower than that of neat $PU_{30}$ (Fig. 3) and approached a higher residue stresses. These results could be explained by observed changes in the morphology of PU brought by filler addition because the stress transfer and relaxation of segments could be quite different through specimens with long thicker fibrils of stretched neat $PU_{30}$ compared to the short thinner fibrilar structure of the $PU+CaCO_3$ nanocomposite.

## FTIR analysis

### Vibrational assignment

The vibrational IR spectra of unstretched samples of $PU_{20}$, $PU_{30}$, and the $PU+CaCO_3$ nanocomposite films are shown in Figures 4 and 5. They show the many characteristic group vibrations of functional groups commonly found in PU polymers. The frequencies of these vibrations are slightly affected by the framework to which a group is bonded. Tentative band assignments were based on the comprehensive analysis of the IR spectra of polyesters,[19] different PUs,[19–27] and isocyanates.[22] The observed vibrational bands and their assignments are presented in Table II.

All the spectra were characterized by the NH stretching vibrations observed in the 3500–3200-$cm^{-1}$ wave-number region. The symmetric and antisymmetric stretching modes of $CH_2$ groups were in the region 3000–2800 $cm^{-1}$. The bands observed between 1480 and 1400 $cm^{-1}$ were attributed to $CH_2$ scissoring vibrations.[28] The weak bands found at 1370 and 1362 $cm^{-1}$ were connected to the wagging vibrations of methylene groups, whereas the band at 1311 $cm^{-1}$ was assigned to $CH_2$ twisting.

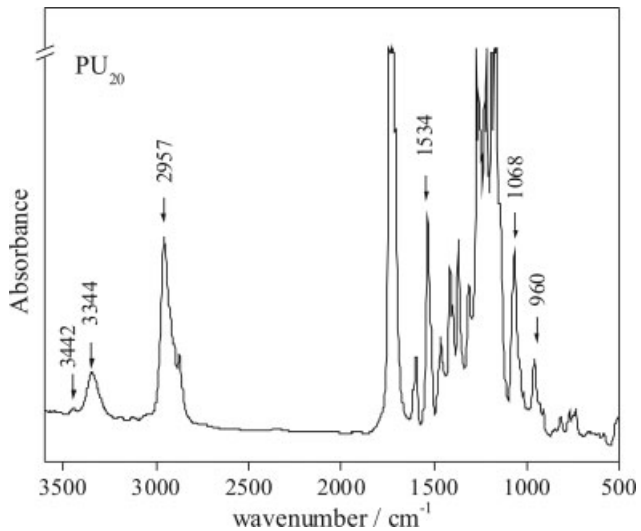


**Figure 4** Absorbance spectrum of the unstretched $PU_{20}$ film.

C=O stretching was the most distinctive absorption band in IR due to its high intensity and the unique range, between 1750 and 1710 $cm^{-1}$, where this vibration occurred. Aromatics display a characteristic C=C stretching at about 1600 $cm^{-1}$, which, in combination with CH stretching above 3000 $cm^{-1}$ (3200–3040 $cm^{-1}$), identifies polymers containing them. The strong band at 1534 $cm^{-1}$ originated from the coupling of CN stretching and NH bending. A review of reported data in the literature suggests that this normal mode is characteristic of 4,4′-methylenedyphenyl diisocyanate (MDI).[20,22]

In the IR spectra of the unstretched PU samples (Figs. 4 and 5), it was not possible to resolve the vibrational bands in the region 1300–1150 $cm^{-1}$ because of the strong absorbance. These vibrational bands were resolved in the IR spectra of highly stretched neat PU and the PU+$CaCO_3$ films. It is known that the bands between 1300 and 1200 $cm^{-1}$ indicated the presence of ester bond vibrations of polyester-based PU.[19]

The IR spectrum of $CaCO_3$ filler was reported in the literature.[29] In the IR spectra of PU+$CaCO_3$, there were bands of the $CaCO_3$ ion $CO_3^{2-}$ observed at 873 and 714 $cm^{-1}$, which were assigned as out-of-plane bending vibrations. The $CO_3^{2-}$ stretching fundamental at 1419 $cm^{-1}$ was not detected in the absorbance spectra of PU+$CaCO_3$ because it was overlapped with normal modes arising from $CH_2$ scissoring vibrations. From the comparison of the IR spectra of neat PU and PU+$CaCO_3$, it was evident there were no chemical interactions between the polymer and filler.

PU was segmented and exhibited a two-phase microstructure consisting of hard segments and soft segments. The analysis of the IR spectra revealed vibrations arising from the different PU segments and suggested that the hard segment of the investigated PU was based on MDI, whereas the soft segment was polyester.

## Hydrogen bonding

In polyester urethane, there is a possibility for the formation of hydrogen bonds between different phases.[17] The NH group from a hard segment donates a proton, whereas the acceptor group is a carbonyl group in either the hard segment (MDI) or in the polyester soft segment. The analysis of the NH and C=O stretching vibrations also yields information about possible interactions between the hard and soft segments in PU polymers. The NH stretching fundamentals are observed between 3500 and 3200 $cm^{-1}$, whereas the region at approximately 1750–1700 $cm^{-1}$ is related to the carbonyl C=O stretching vibrations. In the case of hydrogen bonding, the stretching vibrations are shifted to lower wave numbers. The shift is thus used as an indicator for the existence of hydrogen bonding. The part of the spectrum corresponding to the NH stretching region of $PU_{30}$ is shown in Figure 6. The broad asymmetric band consisted of several overlapping bands. The curve fitting of the NH stretching region gave three Gaussian bands corresponding to vibrations of free and hydrogen-bonded NH groups. The band at 3442 $cm^{-1}$ assigned to stretching vibrations of free NH groups was very low in absorbance.[17] The most intensive band at 3344 $cm^{-1}$ corresponded to the stretching of NH groups hydrogen bonded to carbonyl in the hard segment (hard–hard segment interaction).[17] In the spectra of polyether PU, the band observed at 3295 $cm^{-1}$ was assigned to the

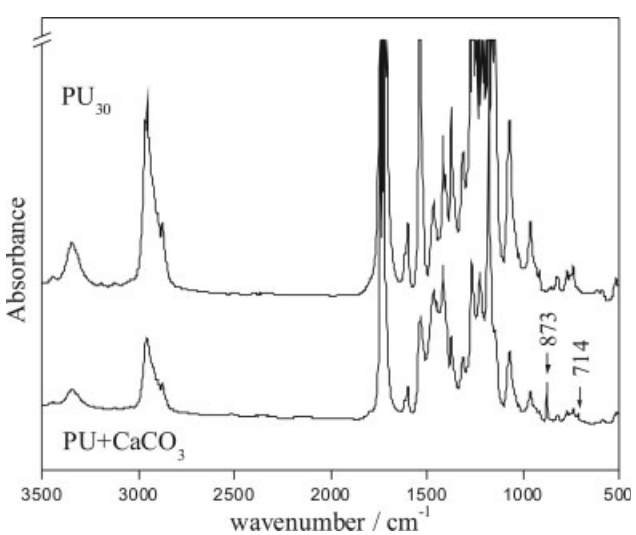


**Figure 5** Absorbance spectra of the unstretched $PU_{30}$ and PU+$CaCO_3$ films.

**TABLE II**
**Assignment of the Observed Vibrational Bands of Neat PU and the PU+$CaCO_3$ Nanocomposite Films**

| Observed bands ($cm^{-1}$) | Relative intensity | Assignment |
|---|---|---|
| 3442 | w | NH stretching (nonbonded) |
| 3344 | m | NH stretching (bonded) |
| 3290 | w | NH stretching (bonded) |
| 3186 | vw | CH stretching (aromatic) |
| 3122 | vw | CH stretching (aromatic) |
| 3043 | vw sh | CH stretching (aromatic) |
| 2957 | s | $CH_2$ stretching |
| 2930 | s | $CH_2$ stretching |
| 2900 | m | $CH_2$ stretching |
| 2876 | m | $CH_2$ stretching |
| 1750–1710 | vs | C=O stretching |
| 1614 | m sh | C=C aromatic stretching |
| 1598 | m | C=C aromatic stretching |
| 1534 | s | CN stretching coupled with NH bending |
| 1514 | w sh | |
| 1476 | w sh | $CH_2$ scissoring |
| 1465 | m | $CH_2$ scissoring |
| 1453 | vw sh | $CH_2$ scissoring |
| 1415 | m | $CH_2$ scissoring |
| 1402 | w | $CH_2$ scissoring |
| 1370 | w | $CH_2$ wagging |
| 1362 | w | $CH_2$ wagging |
| 1320 | w | $CH_2$ twisting |
| 1311 | w | $CH_2$ twisting |
| 1258 | vs | C—O—C stretching (soft segment) |
| 1223 | s | C—C, C—O—C stretching (soft segment) |
| 1205 | s | |
| 1170 | s | C—O—C stretching (hard segment) |
| 1142 | s | C—O—C stretching (hard segment) |
| 1068 | m | C—O—C asymmetric stretching (soft segment) |
| 1042 | w sh | C—O—C symmetric stretching (soft segment) |
| 1018 | vw | CH bending |
| 960 | w | CH bending |
| 936 | vw | CH bending |
| 912 | w | CH bending |
| 873 | m | $CO_3^{2-}$ out-of-plane bending |
| 865 | vw sh | CH out-of-plane bending |
| 852 | w | CH out-of-plane bending |
| 820 | w | CH out-of-plane bending or C=O—C wagging |
| 770 | w | CCO bending |
| 750 | vw | CH out-of-plane bending |
| 736 | w | C=O wagging |
| 722 | vw sh | C=O wagging |
| 714 | vw | $CO_3^{2-}$ out-of-plane bending |
| 617 | vw | C=O wagging, CCC bending |
| 586 | vw | C=O wagging, C=O in-plane bending |
| 510 | vw | CH out-of-plane bending |

s = strong; m = moderate; w = weak; v = very; sh = shoulder.

NH-ether oxygen hydrogen bond with the soft segments.[17] Therefore, the band at 3290 $cm^{-1}$ in the absorbance spectra of $PU_{30}$ was attributed to NH stretching vibrations bonded to the C=O group in the polyester soft segment (hard–soft segment interaction).

Unfortunately, because of its high intensity, the C=O stretching band was observed within the acceptable range only in the highly stretched $PU_{20}$ film (575%) and, even then, only for the parallel polarization. Most of the $CH_2$ and C—O—C groups were present in the soft segments. In the IR spectra of PU and PU+$CaCO_3$, there were bands with very high absorbance values observed at 1258, 1223, 1068, and 1042 $cm^{-1}$ assigned as a stretching vibrations of C—O—C groups. The band at 1068 $cm^{-1}$ assigned as C—O—C vibrations of ester functional groups was correlated with soft-segment orientation behavior.

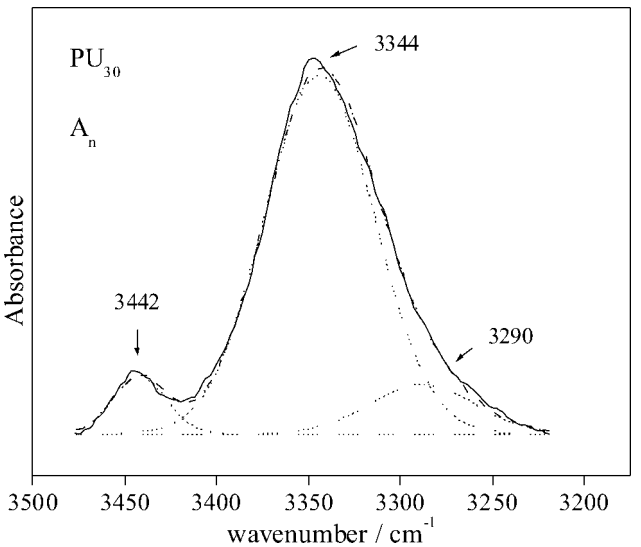


**Figure 6** Absorbance spectrum $A_n(\tilde{v})$ in the NH stretching region of the $PU_{30}$ film stretched transversally to 300%.

The degree of phase domain separation (DPS) of NH and C=O groups in hydrogen bonding was possible to determine from the integrated intensities of the absorbance bands. It depended on hard-segment content, the length of segments, and intra-segment and intersegment interactions such as hydrogen bonding.[7] DPS could be estimated with the following relation:

$$\mathrm{DPS} = \frac{A_{\mathrm{bonded}}}{A_{\mathrm{bonded}} + A_{\mathrm{free}}}$$

where $A_{\mathrm{bonded}}$ and $A_{\mathrm{free}}$ are the intensities of the absorbances of stretching vibrations of hydrogen-bonded and free NH or C=O groups, respectively.[7] The analysis indicated that NH groups in PU and PU+$CaCO_3$ were nearly completely hydrogen bonded (93%), independent of the degree of polymer stretching. Of all the hydrogen bonded NH groups, 85% of them participated in hard–hard segment interaction.

## Orientational behavior of the hard and soft segments

The study of polymers with polarized IR radiation permits the determination of the direction that the transition moment associated with a given normal mode makes with the stretching directions.[30–33] An important parameter that can provide information about the degree of molecular orientations under the influence of ε is the dichroic ratio ($R$), which is defined as

$$R = \frac{A_p}{A_n}$$

where $A_p$ and $A_n$ are the integrated absorbances of the investigated band measured with light polarized parallel and perpendicular, that is, normal to the stretching direction, respectively. The value of $R$ can range from zero (where there is no absorption in the perpendicular direction) to infinity (no absorption in parallel direction). For random orientation of transition moments, $R = 1$; hence, the sample is isotropic. The polarized absorbances $A_p$ and $A_n$ were evaluated from $A_p(\tilde{v})$ and $A_n(\tilde{v})$ by the integration of the respective absorption bands after baseline corrections. The Gaussian functions were fitted to the experimental spectra to separate overlapping bands. Half-widths and intensities were allowed to vary in the iteration process. The maximum error associated with the fit was estimated to be less than 5%.

The orientation of polymer chains under stress can be described by the second moment orientation function:

$$P_2(\cos\vartheta) = \frac{1}{2}\left(3\langle\cos^2\vartheta\rangle - 1\right) = \frac{R_0 + 2}{R_0 - 1}\cdot\frac{R - 1}{R + 2}$$

$P_2(\cos\vartheta)$ in the 2nd order legendxe polynomial in cos $\vartheta$.

where $R_0 = 2ctg^2\alpha$, ($R_0 = 2\cot^2\alpha$) where $\alpha$ is the angle of the transition moment and the chain axis, and $\vartheta$ is the angle between the stretching direction and the local chain axis of the polymer or any directional vector characteristic of a given chain segment. The value of $P_2(\cos\vartheta)$ can be shown to vary from $-½$ for perpendicular alignment ($\vartheta = 90^\circ$) to zero for random chain orientation ($\langle\cos^2\theta\rangle = ⅓$ for random values of $\vartheta$ in spherical polar coordinates) to unity for perfect chain alignment along the draw axis (all $\vartheta = 0$).

When a film is stretched, the chains do not all become oriented in the same direction but assume a distribution of orientations in about this direction. In general, it is not possible to obtain the form of this distribution based only on $R$ measurements. However, some general conclusions about the mechanism of polymer chain alignment can be obtained with a film stretched longitudinally and transversally to the direction of the film axis preparation.

The polarized absorbance spectra of $PU_{20}$ after 300% extension in the transversal direction are shown in Figure 7. It was obvious that the majority of the vibrational bands of PU exhibited linear dichroism. In other words, there was the preferential absorption of one of two mutually perpendicular components of linearly polarized light. The $R$ value of all fundamentals observed in the absorbance spectra of all unstretched samples was nearly 1.0, which suggests that the corresponding transition moments were randomly oriented.

To obtain further information about the relaxation process in the stretched PU and PU+$CaCO_3$ films, we measured the absorbances $A_p$ and $A_n$ immedi-

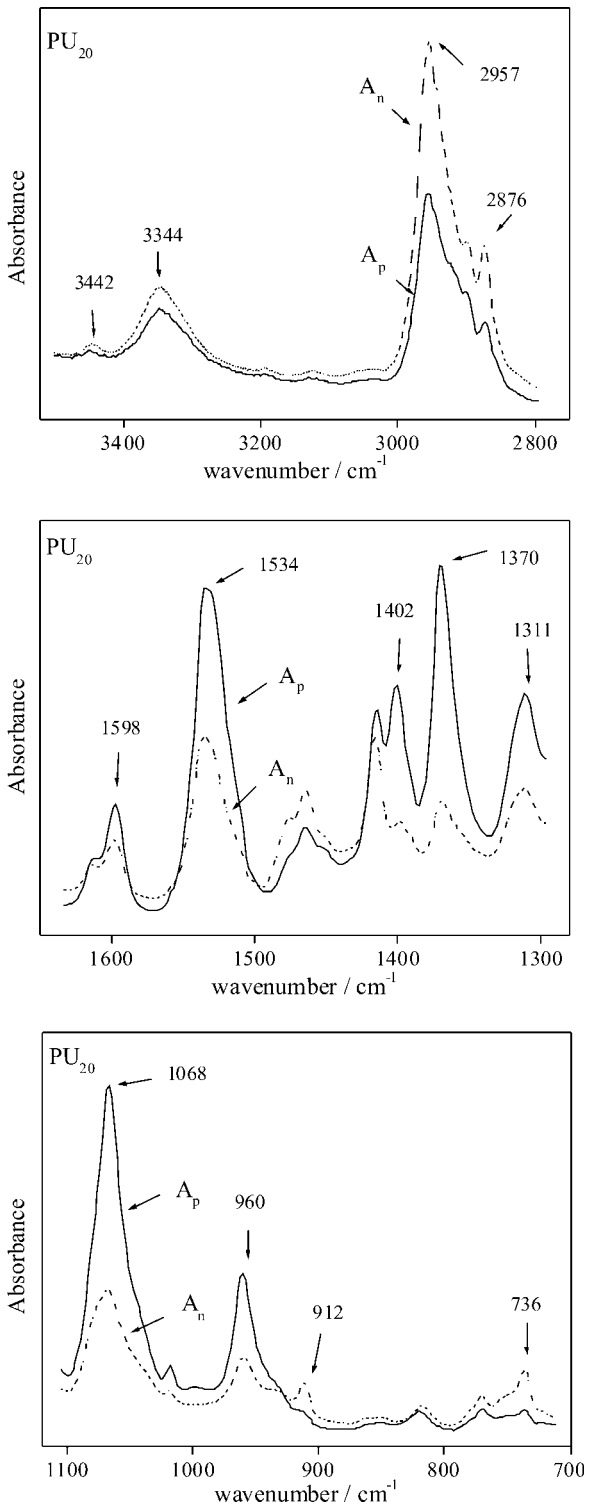


**Figure 7** Polarized absorbance spectra $A_p(\tilde{v})$ and $A_n(\tilde{v})$ of $PU_{20}$ stretched in the transversal direction at 300% elongation.

ately at the end of stretching and then 20 min later. The values of $R$ for the NH stretching bands are presented in Table III. The analysis showed that the orientation of dipole moments changed after stretching and reached constant value after 20 min. The results were consistent with the stress relaxation results.

The factor affecting the stress–ε behavior was the orientation of the hard and soft segments. In the IR spectra (Table II), there were characteristic vibrational bands originating from the different segments. The absorption bands associated with NH and C=O groups in urethane are typically used for hard-segment orientation. The stretching modes of these groups have no coupling with any other vibrational modes, and thus, the angle between the displacement vector of C=O and NH and the main chain are exactly the same as the angle between the transition moment of C=O and NH stretching vibrations and the hard segment. Unfortunately, in the PU samples, the $R$ value of the C=O stretching vibration could not be determined because it was the strongest absorption measurable in transmittance only for the extremely thin sample. Therefore, in our study, the orientational behavior of the hard segments was analyzed with the NH stretching vibrations and C=C phenyl ring vibrations of MDI.

Because the transition moment of the NH stretching is perpendicular to a hard segment ($\alpha = 90^\circ$),[17] the alignment of PU hard segments could be analyzed by the dependence of the orientation function on the ε from the following relation:

$$P_2(\cos \vartheta) = -2 \cdot \frac{R-1}{R+2}$$

At 0% ε, $R = 1.0$, and all hard segments are randomly oriented, which gives the net orientation function $P_2(\cos \vartheta) = 0$.

There were three different hard-segment populations: the first population consisted of the free hard segments embedded in the soft PU matrix, the second population included the hard segments hydro-

**TABLE III**
**Dichroic Ratios of the Neat $PU_{30}$ and PU+$CaCO_3$ Nanocomposite Films**

| NH stretching vibrations ($cm^{-1}$) | ε (%) | $PU_{30}$ longitudinal | | PU+$CaCO_3$ transversal | |
|---|---|---|---|---|---|
| | | $R'$ | $R$ | $R'$ | $R$ |
| 3442 | 0 | 1.055 | 1.184 | 0.929 | 0.912 |
| | 25 | 0.893 | 0.995 | 0.954 | 0.937 |
| | 50 | 1.033 | 0.950 | 0.999 | 0.994 |
| 3344 | 0 | 1.017 | 1.023 | 1.021 | 1.000 |
| | 25 | 0.964 | 0.962 | 0.943 | 0.942 |
| | 50 | 0.901 | 0.884 | 0.885 | 0.880 |
| 3290 | 0 | 1.036 | 1.025 | 1.345 | 1.005 |
| | 25 | 0.960 | 1.038 | 1.075 | 0.986 |
| | 50 | 1.049 | 0.960 | 0.950 | 0.979 |

$R'$ = dichroic ratio immediately after stretching; $R$ = dichroic ratio 20 min after stretching.

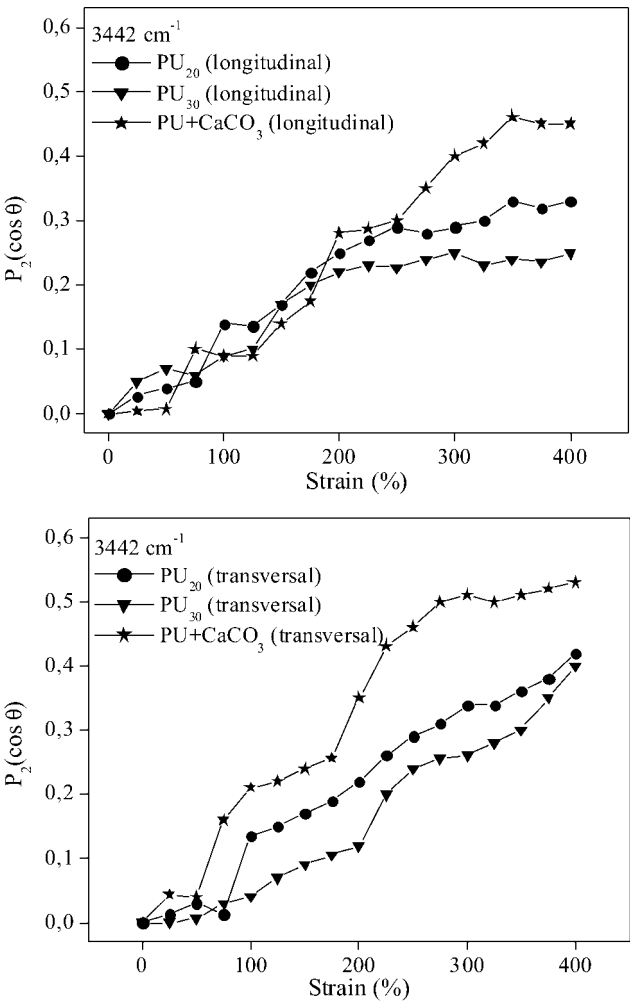


**Figure 8** Comparison of the free-hard-segment orientation in the $PU_{20}$, $PU_{30}$, and PU+$CaCO_3$ films as a function of applied ε.

gen bonded in the hard domains, and the third population corresponded to the hard segments hydrogen bonded to soft segments in the intermediate phase. The population of the free hard segments was characterized by the NH stretching vibration observed at 3442 $cm^{-1}$ (Fig. 6). The transition moment connected with this normal mode was oriented perpendicularly to the stretching direction ($R < 1.0$), so the free hard segments oriented themselves in the stretching direction. There were two different regimes of orientational behavior in the samples stretched longitudinally (Fig. 8). At ε's below 200%, the orientation function showed a very similar linear dependence for all samples. At higher ε's, the increase in orientation was very slow for the neat $PU_{20}$ and $PU_{30}$ films and depended on the film thickness. The alignment of free hard segments was particularly pronounced in the PU+$CaCO_3$ film. Also, there was an appreciable difference in the orientational behavior of films stretched transversally (Fig. 8). There were very slight changes in orientation in the early stage of drawing (ε range = 0–75%); rapid increases then suggested a better alignment of free hard segments, probably due to the lower degree of relaxation in this direction. This result shows that the presence of nanoparticles in the PU+$CaCO_3$ films stretched transversally and longitudinally relative to the film preparation direction enlarged the alignment of free hard segments along the stretching direction. The alignment of free hard segments in the neat PU films was better in thinner sample.

From the analysis of the 3344-$cm^{-1}$ band, which corresponded to hard–hard segment hydrogen bonding, important information about hard-segment orientation due to applied ε could be obtained. According our estimation 85% of NH groups in the hard domains were hydrogen bonded.

The orientation function of all of the investigated samples stretched longitudinally to the direction of film preparation indicated an almost linear increase in the positive orientation of hard segments (Fig. 9).

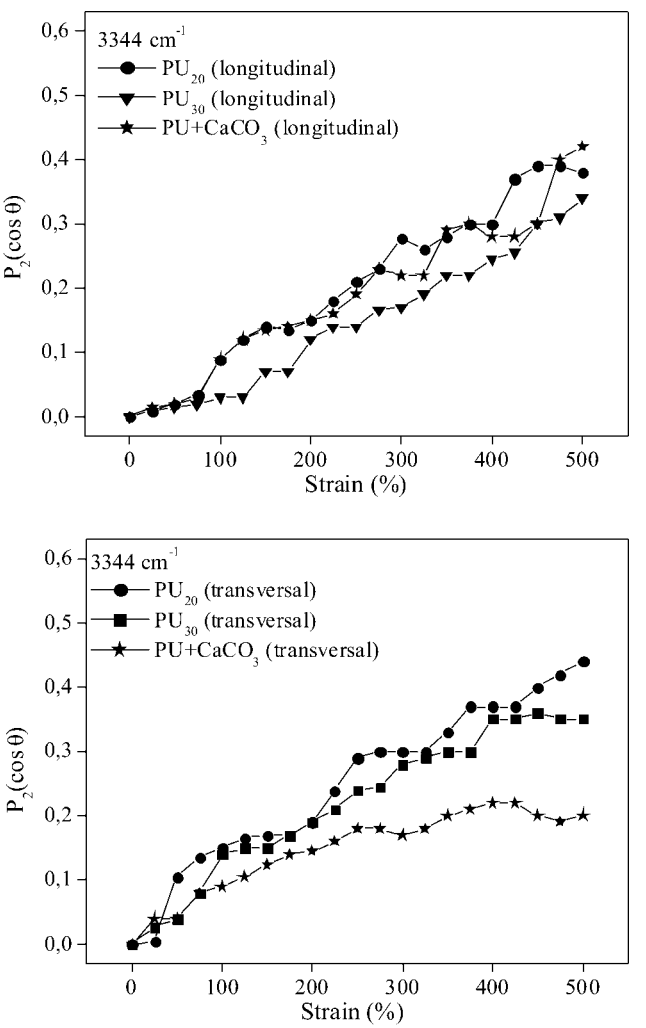


**Figure 9** Variation in the orientation function for hard segments bonded in hard domains on the basis of the NH stretching band at 3344 $cm^{-1}$ upon stretching.

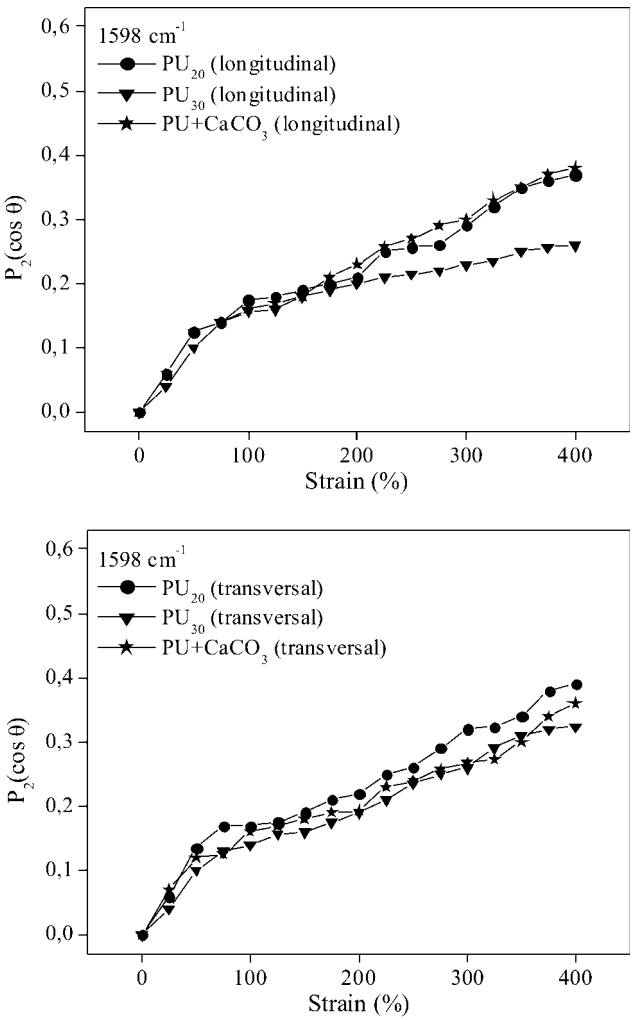


**Figure 10** Orientation function dependence on the applied ε calculated from C=C phenyl stretching.

The results obtained for the PU+$CaCO_3$ film stretched transversally indicate that the addition of filler decreased the orientation ability of the NH stretching transition moments (Fig. 9).

The hard-segment orientation in hard domains were also analyzed with the vibrational bands observed at 1613 and 1598 $cm^{-1}$, which were assigned to the C=C aromatic stretchings of MDI. The transition dipole moment was directed parallel to the hard-segment orientation.[27] The changes in the orientation function of the 1598-$cm^{-1}$ fundamental with ε (Fig. 10) showed parallel alignment of the transition moments connected with the C=C aromatic stretching. According to the orientation function behavior, there was no significant difference in the orientation ability between $PU_{20}$, $PU_{30}$, and PU+$CaCO_3$ films stretched longitudinally and transversally. The band observed at 1613 $cm^{-1}$ showed very similar behavior.

The orientational behavior in PU was very complex because the hard segments could also be hydrogen bonded to polyester soft segments, thus making an intermediate phase.[24] According to our analysis, the band observed at 3290 $cm^{-1}$ was attributed to the stretching of NH groups bonded to C=O groups in the polyester soft segment (hard–soft segment interaction). The values of its $R$ were close to 1.0 in the ε region 0–200%, so the transition moments were randomly oriented. At higher ε's, it was impossible to calculate $R$ because of the very weak intensity of this band. Thus, it was very interesting that the alignment of these hard segments was suggested to have quite different behavior.

The C—O—C stretching mode observed at 1068 $cm^{-1}$ was used to characterize the behavior of the soft segments. The transition moment vector of the C—O—C stretching was taken to be parallel to the chain axis.[24] The orientation function dependence on the applied ε (Fig. 11) suggested an alignment of soft segments along the stretching direction. The degree of orientation in all of the studied samples stretched in the longitudinal and transversal directions showed similar behavior. The alignment was slightly

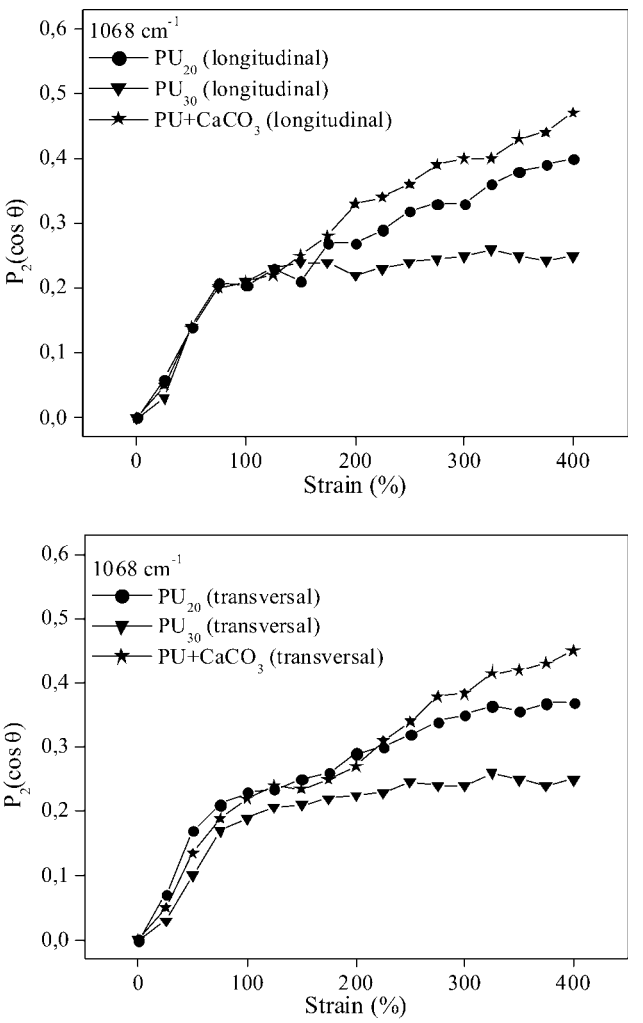


**Figure 11** Soft-segment orientation as a function of applied ε.

greater for longitudinal stretching. The soft segments of the $PU_{20}$, $PU_{30}$, and $PU+CaCO_3$ films showed almost the same linear increase in orientation up to 100% ε. Thereafter, the trends in increasing the degree of soft-segment orientation did not coincide. Above 100% elongation, the orientation function of soft segments in the neat $PU_{20}$ and $PU+CaCO_3$ films continued to linearly increase but with a smaller slope. For neat $PU_{30}$, the value of the orientation function remained almost constant (ca. 0.2) in the stretching region 100–400%.

## CONCLUSIONS

The orientation functions of various functional groups obtained from the IR dichroism study of $PU_{20}$, $PU_{30}$, and the $PU+CaCO_3$ nanocomposite revealed the separation of hard and soft domains and the existence of an intermediate phase. The addition of nanofiller had no influence on the phase separation as seen from the degree of phase separation. The state of well-oriented segments in hard domains was confirmed by the growth of the orientation function of the hydrogen-bonded NH stretching band at 3344 $cm^{-1}$ and the phenyl ring vibrations at 1598 $cm^{-1}$. The alignment of segments in the hard domains and in the intermediate phase was not affected significantly by the film thickness and the presence of nanoparticles.

The analysis of the orientation function of the 1068-$cm^{-1}$ band of the $PU+CaCO_3$ nanocomposite and the thinner $PU_{20}$ films revealed very similar orientational properties of the soft segments. The decrease in ε-induced hardening as confirmed in the stress–ε measurements was connected with the strong alignment of soft segments. Slightly different mechanical properties of films stretched in the longitudinal and transversal directions were confirmed by tensile, stress relaxation, and IR measurements.

## References


1. Lee, Y. M.; Lee, J. C.; Kim, B. K. Polymer 1994, 35, 1095.
2. Tsen, W. C.; Chuang, F. S. J Appl Polym Sci 2006, 101, 4242.
3. Hybrid Materials: Synthesis, Characterization and Applications; Kickelbick, G., Ed.; Wiley-VCH: Weinheim, 2007.
4. Kickelbick, G. Prog Polym Sci 2003, 28, 83.
5. Perez, L. D.; Giraldo, L. F.; Brostow, W.; Lopez, B. L. e-Polymers [Online] 2007, 029.
6. Zheng, J.; Ozisik, R.; Siegel, R. W. Polymer 2006, 47, 7786.
7. Vega-Baudrit, J.; Navarro-Banon, V.; Vasquez, P.; Martin-Martinez, J. M. Int J Adhes Adhes 2006, 26, 378.
8. Dan, C. H.; Lee, M. H.; Kim, Y. D.; Min, B. H.; Kim, J. H. Polymer 2006, 47, 6718.
9. Pattanayak, A.; Jana, C. S. Polymer 2005, 46, 5183.
10. Chen, T.-K.; Tien, Y.-I.; Wei, K.-H. Polymer 2000, 41, 1345.
11. Nunes, R. C. R.; Fonseca, J. L. C.; Pereira, M. R. Polym Test 2000, 19, 93.
12. Lučić Blagojević, S.; Kovačević, V.; Leskovac, M.; Vrsaljko, D.; Volovšek, V.; Nover, C. e-Polymers [Online] 2004, 036.
13. Sawyer, L. C.; Grubb, D. T. Polymer Microscopy; Chapman & Hall: London, 1996.
14. Manias, E.; Polizos, G.; Nakajima, H.; Heidecker, M. J. In Flammability of Polymer Nanocomposites; Wilkie, C.; Morgan, A., Eds.; Wiley: New York, 2007.
15. Christenson, E. M.; Anderson, J. M.; Hiltner, A.; Baer, E. Polymer 2005, 46, 11744.
16. Tanniru, M.; Misra, R. D. K. Mater Sci Eng A 2006, 424, 53.
17. Petrović, Z. S.; Ferguson, J. Prog Polym Sci 1991, 16, 695.
18. Ward, I. M. Mechanical Properties of Solid Polymers, 2nd ed.; Wiley: New York, 1983.
19. Mishra, A. K.; Chattopadhyay, D. K.; Sreedhar, B.; Raju K. V. S. N. Prog Org Coat 2006, 55, 231.
20. Ciobanu, C.; Ungureanu, M.; Ignat, L.; Ungureanu, D.; Popa V. I. Ind Crops Prod 2004, 20, 231.
21. Irusta, L.; Fernandez-Berridi, M. J. Polymer 2000, 41, 3297.
22. Yilgor, I.; Yilgor, E.; Guclu Guler, I.; Ward, T. C.; Wilkes, G. L. Polymer 2006, 47, 4105.
23. Siesler, H. W. Pure Appl Chem 1985, 57, 1603.
24. Kim, H.-J.; Worley, D. C.; Benson, R. S. Polymer 1997, 38, 2609.
25. Lee, H. S.; Ko, J. H.; Song, K. S.; Choi, K. H. J Polym Sci Part B: Polym Phys 1997, 35, 1821.
26. Schoonover, J. R.; Dattelbaum, D. M.; Osborn, J. C.; Bridgewater, J. S.; Kenney, J. W. Spectrochim Acta A 2003, 59, 309.
27. Melnig, V.; Tura, A. V.; Ciobanu, C. J Membr Sci 2005, 267, 58.
28. Bistričić, L.; Volovšek, V.; Dananić, V.; Movre Šapić, I. Spectrochim Acta A 2006, 64, 327.
29. Gilbert, M.; Sutherland, I.; Guest, A. J Mater Sci 2000, 35, 391.
30. Thulstrup, E. W.; Michl, J. Elementary Polarization Spectroscopy; Wiley-VCH: New York, 1989.
31. Bokobza, L. Anal Sci 2001, 17, 675.
32. Schoonover, J. R.; Thompson Graff, D.; Osborn, J. C.; Orler, E. B.; Wroblenski, D. A.; Marsh, A. L.; Wang, H.; Palmer, R. A. Polym Degrad Stab 2001, 74, 87.
33. Nair, B. R.; Gregoriou, V. G.; Hammond, P. T. Polymer 2000, 41, 2961.